AGU PUBLICATIONS

JGR

Journal of Geophysical Research: Planets

COMMENTARY
10.1002/2016JE005150

**Special Section:**
JGR-Planets 25th Anniversary

**Key Points:**
- MESSENGER discovered that Mercury is a far more dynamic planet than previously recognized
- Mercury's earliest history was marked by vigorous interior and surface geological activity
- Modern-day Mercury has a dynamic space environment that is coupled to an active core dynamo and that interacts with the surface

**Correspondence to:**
C. L. Johnson,
cjohnson@eos.ubc.ca

**Citation:**
Johnson, C. L., and S. A. Hauck, II (2016), A whole new Mercury: MESSENGER reveals a dynamic planet at the last frontier of the inner solar system, *J. Geophys. Res. Planets*, *121*, 2349–2362, doi:10.1002/2016JE005150.

Received 3 AUG 2016
Accepted 28 SEP 2016
Accepted article online 30 SEP 2016
Published online 2 NOV 2016



# A whole new Mercury: MESSENGER reveals a dynamic planet at the last frontier of the inner solar system

**Catherine L. Johnson[1,2] and Steven A. Hauck, II[3]**

[1]Department of Earth, Ocean and Atmospheric Sciences, University of British Columbia, Vancouver, British Columbia, Canada, [2]Planetary Science Institute, Tucson, Arizona, USA, [3]Department of Earth, Environmental, and Planetary Sciences, Case Western Reserve University, Cleveland, Ohio, USA

## Abstract

The MErcury Surface, Space ENvironment, GEochemistry, and Ranging (MESSENGER) mission yielded a wealth of information about the innermost planet. For the first time, visible images of the entire planet, absolute altimetry measurements and a global gravity field, measurements of Mercury's surface composition, magnetic field, exosphere, and magnetosphere taken over more than four Earth years are available. From these data, two overarching themes emerge. First, multiple data sets and modeling efforts point toward a dynamic ancient history. Signatures of graphite in the crust suggest solidification of an early magma ocean, image data show extensive volcanism and tectonic features indicative of subsequent global contraction, and low-altitude measurements of magnetic fields reveal an ancient magnetic field. Second, the present-day Mercury environment is far from quiescent. Convective motions in the outer core support a modern magnetic field whose strength and geometry are unique among planets with global magnetic fields. Furthermore, periodic and aperiodic variations in the magnetosphere and exosphere have been observed, some of which couple to the surface and the planet's deep interior. Finally, signatures of geologically recent volatile activity at the surface have been detected. Mercury's early history and its present-day environment have common elements with the other inner solar system bodies. However, in each case there are also crucial differences and these likely hold the key to further understanding of Mercury and terrestrial planet evolution. MESSENGER's exploration of Mercury has enabled a new view of the innermost planet, and more importantly has set the stage for much-needed future exploration.

## Plain Language Summary

The recent investigation of the planet Mercury by NASA's MESSENGER mission has resulted in a wealth of new discoveries. Now there are high-resolution pictures of the entire planet that permit characterization of the geology of the planet. Further, there are measurements of topography, of gravity variations across the surface that indicate the structure of the subsurface, of the magnetic field that reveal how the planet interacts with the solar wind and how its deep interior has evolved, of the chemical composition of the rocks of the surface, and of the extended atmosphere (exosphere). We now have a view of Mercury that is quite different from the one that prevailed prior to MESSENGER's arrival at the planet. Rather than a long-quiet relic from the era of planet formation, Mercury has been a dynamic planet for most, if not all of its lifetime. Indeed, the data from MESSENGER contain signs of an ocean of magma covering the surface in the planet's earliest history and a billion years of voluminous volcanism that followed, as well as the generation of a magnetic field in its core in that same era. Further, modern Mercury has a magnetic field unique among the planets, exhibits variations in the character of its exosphere, and shows signs of activity such as the existence of water ice at the poles and loss of rock to space in enigmatic surface features termed hollows. Each new discovery has revealed new questions about the planet that collectively argue for continued exploration of the innermost planet.

## 1. Introduction

The proximity of the innermost planet to the Sun makes it challenging to observe from Earth and to explore with spacecraft. As a result, until recently Mercury has effectively remained the last frontier of discovery within the inner solar system. In 2011, the MErcury Surface, Space ENvironment, GEochemistry, and

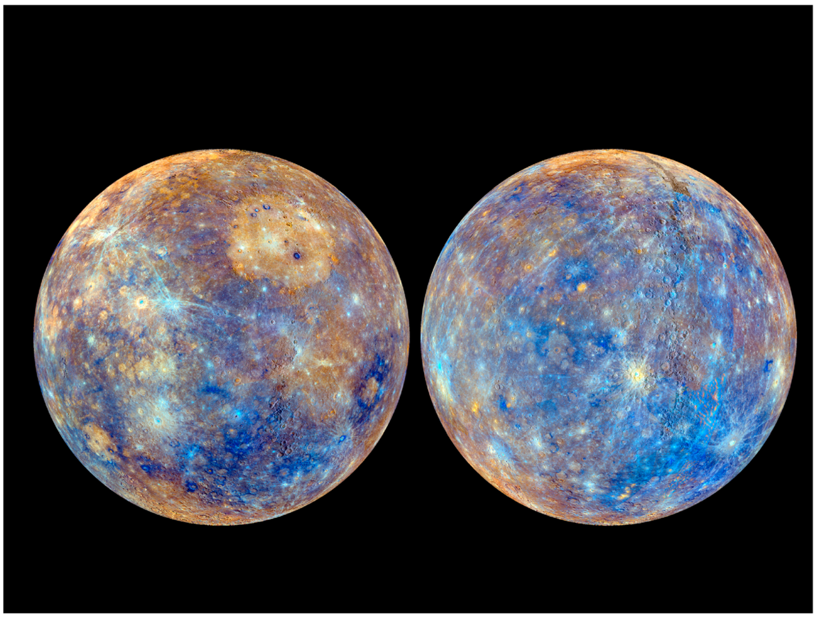

**Figure 1.** Enhanced color composite images of Mercury from the Wide Angle Camera of the Mercury Dual Imaging System. Images are hemispheres centered on the equator and longitudes (left) 140°E and (right) 320°E. Different colors reflect different chemical and physical properties of the surface units. Young, fresh impact craters and rays extending radially from them, appear light blue or white. Tan areas are plains units, dominantly of volcanic origin. The Caloris basin is the large circular tan feature located just to the upper right of center of the left image. Medium- and dark-blue areas are the low-reflectance material (LRM), thought to be enriched in graphite. Patches of LRM often occur as terrain within craters (e.g., some of the craters within the Caloris basin).

Ranging (MESSENGER) spacecraft became the first spacecraft to orbit Mercury. The four years of orbital operations, combined with three flybys in 2008 and 2009, have enabled fundamental discoveries including, at long last, visible images of the entire planet (Figure 1). In this commentary, we report on some of the key scientific results from the MESSENGER mission. We focus on discoveries that have contributed to a new global picture of the present-day planet and its early history.

Earth-based telescopic and radar observations of Mercury have provided basic information on the planet's size (Figure 2), orbital and rotational characteristics [e.g., *Pettengill and Dyce*, 1965]. The Mariner 10 spacecraft flew by Mercury 3 times in 1974–1975, providing in situ views of about 45% of the planet and revealing a crater-dominated surface (Figure 1). The description of Mercury as a small, airless, cratered planet has often led to comparisons with the Moon despite the very different origin and interior structure of these two bodies. Mariner 10 estimates of Mercury's mass implied a metallic core with radius 72–90% of the planetary radius [*Harder and Schubert*, 2001; *Hauck et al.*, 2007], compared with ~55% for Earth (Figure 2), Venus, and Mars, and ~20% for the Moon. The origin of Mercury's high metal-to-silicate ratio that resulted in such a fractionally large metallic core was a major outstanding question, intimately linked to the planet's formation and evolution. Other, complementary constraints on the bulk composition of the planet [e.g., *Taylor and Scott*, 2003], and the possible existence of an early magma ocean and floatation crust [e.g., *Brown and Elkins-Tanton*, 2009], were minimal. Furthermore, estimates of the thickness of the crust [e.g., *Nimmo*, 2002; *Nimmo and Watters*, 2004] were limited by the absence of global gravity and topography data sets typical of other inner solar system bodies. Several other issues arose related to the thermal and tectonic evolution of the planet. First, the origin of the so-called smooth (less heavily cratered) plains units was unknown—both volcanic and impact-related explanations were proposed [e.g., *Strom et al.*, 1975; *Wilhelms*, 1976]. Second, long lobate scarps seen in Mariner 10 images indicated global contraction of 1–2 km over the past 4 billion years [*Strom et al.*, 1975; *Watters et al.*, 1998] and led to a decades-long puzzle of how to reconcile this observation with the cooling of the planet [e.g., *Solomon*, 1977; *Schubert et al.*, 1988; *Hauck et al.*, 2004]. Third, the detection of a weak planetary magnetic field [*Ness et al.*, 1974] was perplexing: challenges were associated with either a core dynamo or crustal origin [*Connerney and Ness*, 1988; *Schubert et al.*, 1988; *Aharonson et al.*, 2004].

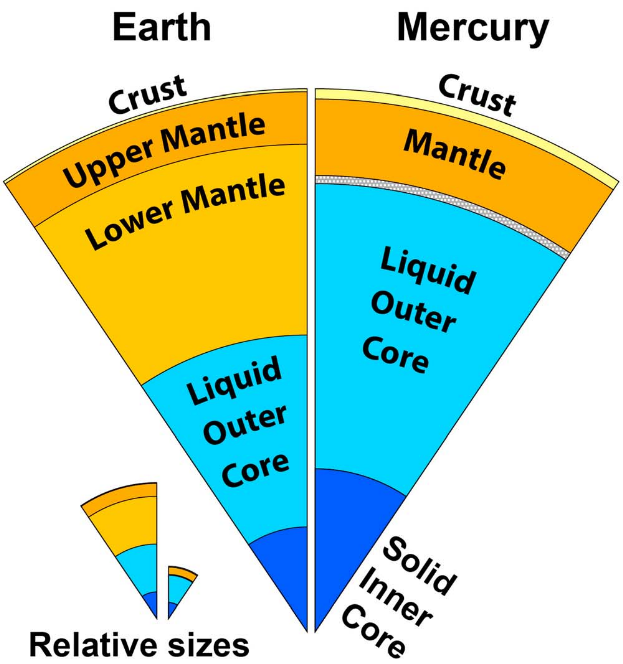


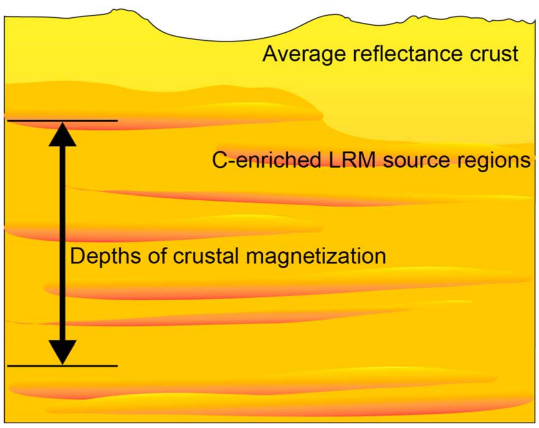


**Figure 2.** (top) A comparison of the internal structure of Mercury and the Earth. Mercury's large bulk density is a reflection of its large metallic core compared to its silicate mantle and crust. The size of Mercury's inner core is unknown, but potentially quite small [*Peale et al.*, 2016]. Together, the MESSENGER-derived gravity field and Earth-based radar observations have enabled the determination of Mercury's core radius, $R_C = 2020 \pm 30$ km, ruling out the pre-MESSENGER canonical value of 1800 km. It has also been suggested that Mercury may possess a distinct solid layer between the liquid outer core and the mantle (hatched pattern) [*Hauck et al.*, 2013]. Inset shows the internal structures of Earth and Mercury to scale. One Mercury radius is $R_M = 2440$ km. (bottom) A schematic representation of possible crustal structure with the sources of LRM distributed throughout the deeper crust and available for exposure and redistribution by impacts. Crustal magnetic fields suggest that very shallow crustal magnetizations are weaker than those at midcrust or greater depths [*Johnson et al.*, 2016].

The presence of a weak planetary magnetic field, but no atmosphere, suggested an intriguing and unique environment above the planet's surface. Mariner 10 data indicated that the planetary field "stands-off" the solar wind, yielding a magnetosphere (the region within which the planetary field is confined and the solar wind is largely excluded) that is a miniature, yet more time-variable, version of its terrestrial counterpart [*Russell et al.*, 1988]. Traces of hydrogen, helium, and oxygen were detected around the planet [e.g., *Broadfoot et al.*, 1974]. Subsequent Earth-based telescopic observations revealed a thin sodium and potassium "exosphere" that varied in time and location [*Potter and Morgan*, 1985, 1986]. Other species were expected but were not detectable from Earth. Although invisible to the naked eye, the magnetosphere and exosphere were suspected to be highly dynamic but the nature of these dynamics and their interactions with the surface and possibly the interior were unknown. For example, whether low-latitude regions of the dayside surface are ever exposed to the solar wind was debated, together with the potential consequences for space weathering of the surface and generation of the exosphere. An inventory of exospheric species, their dynamics, and any links to the planet's surface composition remained to be discovered. Furthermore, there was puzzling evidence for radar-bright circular regions near the poles [e.g., *Slade et al.*, 1992; *Harmon and Slade*, 1992; *Harmon et al.*, 2011]. Thermal model calculations [*Paige et al.*, 1992; *Ingersoll et al.*, 1992] and Earth-based radar data suggested that the observations could be explained in terms of water ice deposits at least several meters deep [*Butler et al.*, 1993], trapped in permanently shadowed regions of high-latitude craters. Unresolved issues included a definitive demonstration that the radar-bright material was indeed water ice, and if so its origin and longevity (i.e., whether these regions are in permanent shadow).

The MESSENGER mission was launched in 2004, with six driving science questions: (1) Why is Mercury so dense? (2) What is the geological history of Mercury? (3) What is the nature of Mercury's magnetic field? (4) What is the structure of Mercury's core? (5) What are the unusual materials at Mercury's poles? (6) What volatiles are important at Mercury? Here we touch on MESSENGER-driven discoveries that address some of these questions, focusing our commentary on the emergence of Mercury as a dynamic planet. We concentrate on two salient themes—Mercury's earliest history and its modern-day dynamic environment.

## 2. A Dynamic Start for the Smallest Planet

The details of the earliest history of any planet are the most difficult to read. The present-day surface geology is the result of processes that have reworked the crust in their own image. Clues to Mercury's early years are recorded in the varying composition of the rocks at the surface (Figure 1), the thickness and distribution of the crust, the magnetization of that crust, and the distribution of large impact craters on the surface.

The processes of formation and earliest differentiation determine a planet's first-order interior structure and set the stage for its subsequent evolution. In this regard, Earth, Venus, and Mars appear similar to each other, but different from both Mercury and the Moon (Figure 2). While the origin of Mercury's high metal-to-silicate ratio is still unknown, MESSENGER results have enabled a whole class of scenarios to be ruled out, namely, those that involve surface temperatures high enough to vaporize silicate materials, incompatible with the current surface volatile inventory of the planet [*Peplowski et al.*, 2011].

As a result of the heat generated by impacts during accretion, metal-silicate differentiation, and high rates of radiogenic heat production, terrestrial bodies experience an early stage where molten rock extends to great depth within the planet, termed a magma ocean. The extensive lunar highlands, that comprise plagioclase-rich anorthosite, are primary evidence of this process on the Moon [*Wood et al.*, 1970]. These rocks floated to the top of the lunar magma ocean because they were less dense than the magma. Experimental determination of the density of magmas consistent with the major element compositions of Mercury's surface indicates that the only mineral capable of floating to the top of a magma ocean there is graphite [*Vander Kaaden and McCubbin*, 2015]. Should Mercury have as much bulk carbon as CI chondrites such a graphite floatation crust could be up to 20 km thick, though a more C-depleted mantle, similar to Mars or Earth, would lead to a crust ~1–100 m thick [*Vander Kaaden and McCubbin*, 2015]. Many impact craters on Mercury appear to excavate relatively low reflectance material (LRM) [e.g., *Denevi et al.*, 2009; *Murchie et al.*, 2015] from several kilometers below the surface (Figure 1). A combination of neutron spectroscopy from low-altitude observations by the MESSENGER spacecraft and visible to near-IR data [*Peplowski et al.*, 2016] indicates that LRM contains 1–3% more carbon than surrounding materials. Exhumation of materials enhanced in graphite at this level from depth is consistent with the idea of a deeper portion of the crust containing remnants of an initial floatation crust that was mixed with later silicate additions to the crust via magmatic assimilation and impact disruption and mixing (Figure 2).

Generation of the later silicate crust was a notably efficient process compared to the other terrestrial planets. Estimates of the average thickness of the crust on Mercury are on the order of 35 km [*James et al.*, 2015; *Padovan et al.*, 2015]. When this value is normalized by the relatively small mantle thickness [*Hauck et al.*, 2013; *Rivoldini and Van Hoolst*, 2013], Mercury's crust is a fractionally larger component of the silicate exterior of the planet than the crust of any other terrestrial planet (or Earth's moon) [*Padovan et al.*, 2014]. Such efficient crust formation implies that magma production rates were quite large early in the planet's history. This conclusion is also consistent with inferences of the large partial melt fractions (up to 50%) responsible for the compositions of the Mg-rich ultramafic rocks [*Stockstill-Cahill et al.*, 2012; *Charlier et al.*, 2013; *Namur et al.*, 2016] that are observed at the surface by X-ray fluorescence spectroscopy [e.g., *Nittler et al.*, 2011; *Weider et al.*, 2015]. Indeed, *Namur et al.* [2016] find that the largest inferred melt fractions and melting temperatures are associated with the oldest terrains, with cooling of up to 70 K per 100 million years inferred between 4.2 and 4.0 Ga. Continued melt fractions of more than 25% are inferred for the more recent 3.7–4.0 Ga lavas. Intriguingly, Mercury shows evidence for vigorous melt production and high temperatures indicating decompression-driven melting [*Michel et al.*, 2013; *Tosi et al.*, 2013], yet geographical variations in the

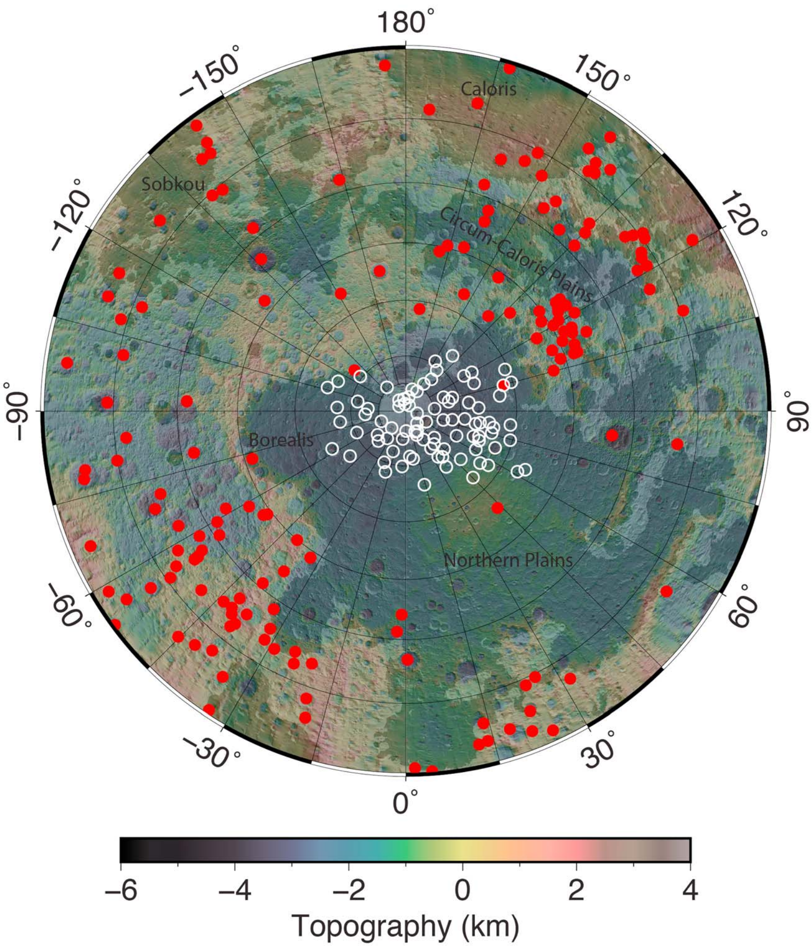


**Figure 3.** Topography of part of Mercury's northern hemisphere (30°N to 90°N) from the Mercury Laser Altimeter, underlain by a map of volcanic plains (darker hues for any given color), showing locations of hollows (red [*Thomas et al.*, 2014]), and craters greater than 10 km in diameter for which at least part of the interior is both in permanent shadow and is radar bright (white open circles [*Chabot et al.*, 2012; *Deutsch et al.*, 2016]). Lambert azimuthal equal area projection centered on the North pole, with grid lines 10° in latitude and 15° in longitude. A few of the major physiographic features are labeled. The Caloris basin (diameter ~1540 km) is centered on 170.2°E and 30.5°N and notably shows elevated topography in its northern interior.

composition of surface rocks also indicate compositionally heterogeneous mantle source regions [e.g., *Charlier et al.*, 2013; *Namur et al.*, 2016]. This duality raises an important question: how was Mercury's mantle convection both vigorous enough to produce a thick crust via high degrees of partial melting but also retain compositionally distinct domains that were not mixed during that convection? The answer may reside in part in Mercury's very thin mantle that could have permitted styles of convection different from those in the mantles of other inner solar system bodies. For example, convective cells could have remained quite localized, resulting in less efficient horizontal mixing.

Further evidence for Mercury's dynamic early history was discovered late in MESSENGER's mission when the spacecraft made observations from vantage points substantially closer to the planet than during the primary mission phase. These orbits permitted the detection of low-amplitude magnetic anomalies [*Johnson et al.*, 2015], the sources of which reside within magnetized rocks in the lithosphere. Although some of this magnetization may be induced in the present or recent field, calculations indicate that at least part of it was acquired as the host rocks cooled below their Curie temperature in the presence of an internally generated magnetic field prior to 3.7 Ga [*Johnson et al.*, 2015]. Thus, MESSENGER has demonstrated that Mercury not only has a field today [e.g., *Anderson et al.*, 2008] but had one in the past as well [*Johnson et al.*, 2015; *Hood et al.*, 2015, 2016]. The high temperatures inferred for the interior from surface materials that date to that period

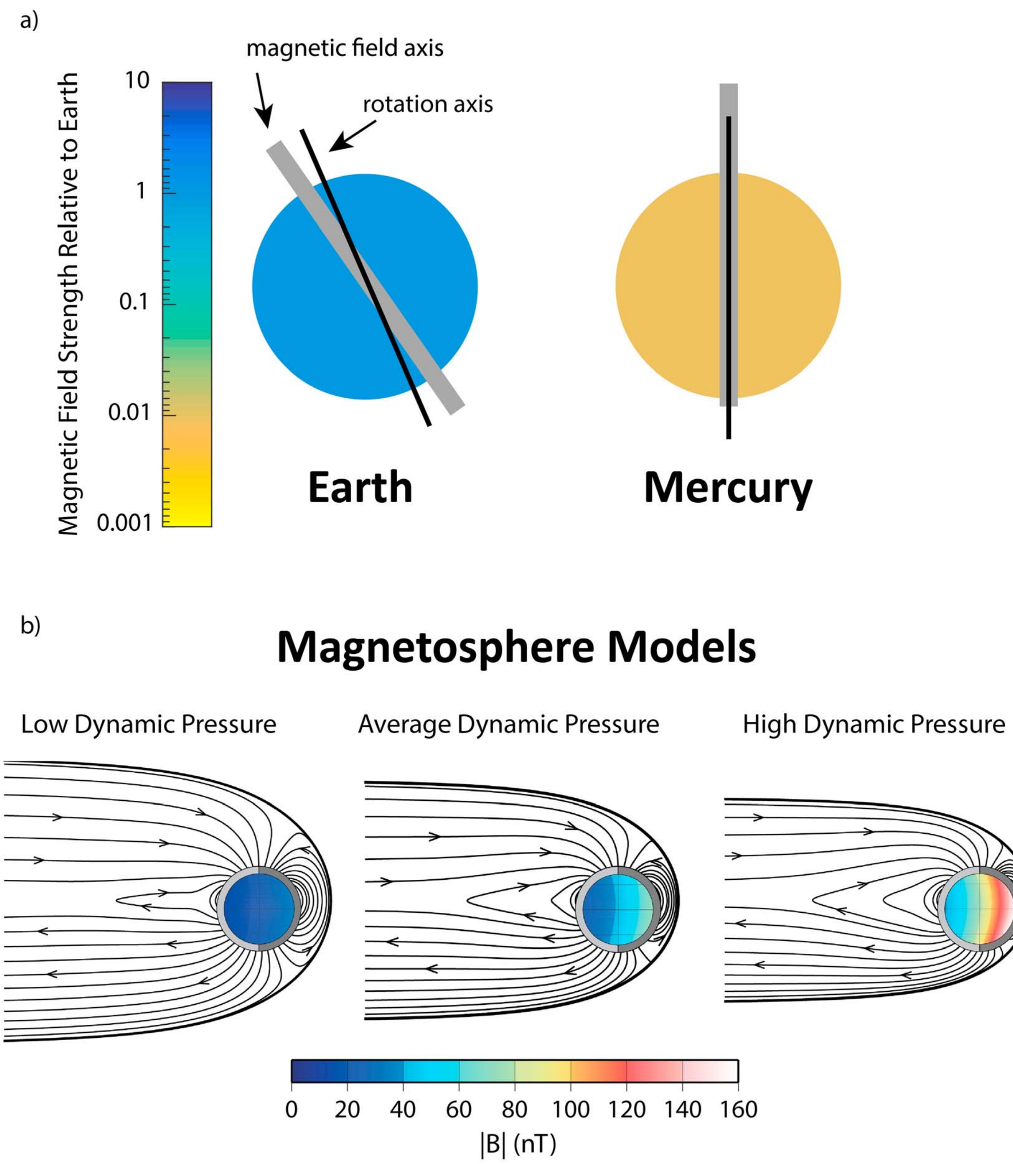


**Figure 4.** (a) Schematic showing the average relative surface strengths and dipole geometries of the internal dynamo fields of Earth and Mercury. For each planet the solid line denotes the spin axis orientation relative to the orbit normal (vertical) and the gray bar denotes the magnetic dipole orientation which for Earth is geocentric, and for Mercury is offset northward by ~0.2 $R_M$. For reference, Earth's field strength at the magnetic equator is ~30,000 nT. (b) Model for Mercury's magnetosphere [*Korth et al*., 2015]. Field lines inside the magnetosphere in the noon-midnight plane are shown and include contributions from the offset axial dipole, magnetopause, and tail fields. Dayside is to the right in each panel. The middle figure shows the average shape and size of the magnetosphere over the duration of the MESSENGER mission (relative to the gray circle denoting the planet), corresponding to a subsolar magnetopause position that is 0.43 $R_M$ above the surface of the planet. The left figure corresponds to lower solar wind pressure conditions when the subsolar magnetopause is farther from the planet (0.7 $R_M$) and the right figure to higher solar wind pressures when the subsolar magnetopause is 0.2 $R_M$ above the planet. During one Mercury year the magnetopause varies by about ±0.1 $R_M$ about its mean position, and during extreme conditions it reaches the surface of the planet or is more than 2 $R_M$ above the surface of the planet. In each figure the field strength that results from the magnetopause fields at the surface of Mercury's core is shown in color (scale bar in nanotesla). The compression and expansion of the magnetosphere lead to time variations in the magnetic field strength at Mercury's core-mantle boundary that in turn induce fields in the core [*Johnson et al*., 2016].

[*Namur et al.*, 2016] and the substantial amount of alloying elements in the core implied by the relatively low core density [*Hauck et al.*, 2013; *Rivoldini and Van Hoolst*, 2013; *Knibbe and van Westrenen*, 2015] suggest that thermally driven convection in the core was responsible for the magnetic field at that time. There is now evidence for crustal magnetization and ancient global magnetic fields on all inner solar system bodies except Venus. An ancient field is not precluded on Venus; the average surface age of less than 1 Gyr [e.g., *McKinnon et al.*, 1997] suggests that the evidence could simply have been erased through destruction and/or reheating of the lithosphere. While Mars and the Moon appear to have had magnetic fields confined to their early history [e.g., *Lillis et al.*, 2008; *Weiss and Tikoo*, 2014], Earth and Mercury both have fields today. Understanding the longevity of Mercury's field, whether it has been continuous in duration, like that of Earth, or intermittent, the driving mechanisms for the dynamo through time, and the mineralogy of the rocks hosting the crustal magnetic field remain open questions.

Although Mercury has orbited the Sun for more than 4.5 billion years, one of its most obvious signs of being a dynamic and active planet, volcanism, appears to be primarily relegated to regions of the planet more than 3.7 billion years old. The largest expanses of volcanic plains [e.g., *Denevi et al.*, 2013; *Ostrach et al.*, 2015] are within and surrounding the Caloris impact basin and northern smooth plains (Figure 3). While there is no obvious crustal dichotomy as on Mars and the Moon, smooth plains volcanism preferentially occurred in the northern hemisphere. Younger effusive volcanism is extremely limited [e.g., *Prockter et al.*, 2010] and associated with impact basins [*Byrne et al.*, 2016], and small-scale explosive volcanism is distributed through time [*Thomas et al.*, 2014]. Impact crater densities on Mercury suggest that volcanism re-worked a notable portion of the surface 4.0–4.1 billion years ago, a time period consistent with the beginning of the Late Heavy Bombardment (LHB) [*Marchi et al.*, 2013]. The interval between the LHB and 300 to 400 million years later is a critical period in Mercury's history during which volcanism that created the thick crust apparently declined rapidly and almost completely. Whether that volcanic shutdown came as a result of the waning of energy imparted by impacts [*Marchi et al.*, 2013], and/or a natural decrease in heat output and convection to produce magma [e.g., *Tosi et al.*, 2013], or was perhaps frustrated in its ability to access the surface due to an increasingly compressive stress environment due to global contraction [e.g., *Solomon*, 1977] remains to be unraveled. With Mercury's contraction (Figure 3) now estimated to be 5–7 km [*Byrne et al.*, 2014] the planet has developed a significant compressional state, which likely started early in its history.

## 3. Modern-Day Mercury Inside and Out: Not Quite so "Dead"

Although modern-day Mercury is geologically quiescent, the near-surface environment is extraordinarily dynamic and couples in surprising ways to the planet itself. Furthermore, evidence for a dynamic deep interior is provided by Mercury's magnetic field. MESSENGER flybys confirmed the detection of a global field and established it to be of core origin [*Anderson et al.*, 2008], indicating convection sufficiently vigorous to power a dynamo. MESSENGER orbital observations showed that the field is not only weak (a surface field strength ~1% that of Earth's) but is highly symmetric about the rotation axis (Figure 4) and asymmetric about the planetary equator—stronger in the northern hemisphere than in the southern hemisphere [*Anderson et al.*, 2011, 2012; *Johnson et al.*, 2012]. These properties render Mercury's field unique among planets in the solar system with present-day dipole-dominated fields (Earth, Saturn, and Jupiter). Mercury's field is similar in its axisymmetry to that of Saturn but is far more equatorially asymmetric and is more than 2 orders of magnitude weaker than the fields of Saturn and Earth. The strength, axisymmetry, and equatorial asymmetry are challenging to simultaneously explain with current dynamo models. A key to understanding the unusual magnetic field may be the type(s) and distributions of light elements in core [e.g., *Stanley and Glatzmaier*, 2010] compatible with inferences of Mercury's bulk and surface composition [*Chabot et al.*, 2014]. Core light element distributions are important because they may control the source(s) of buoyancy that drive convection. Some recent dynamo models have successfully predicted both a low strength and strongly equatorially asymmetric field [*Cao et al.*, 2014; *Tian et al.*, 2015]. However, challenges remain; e.g., the lateral variations in core-mantle boundary heat flow currently required by such models are not expected for the present-day thermal state of the lowermost mantle.

The weak global field with its unusual geometry, as well as the solar wind conditions at Mercury's heliocentric distance, has important consequences for the small magnetosphere. Reconnection of the planetary field with the interplanetary magnetic field (IMF) can occur under almost all IMF conditions [e.g., *DiBraccio et al.*, 2013]. This is unlike at Earth where the strong internal field and weaker IMF restrict reconnection to times when the

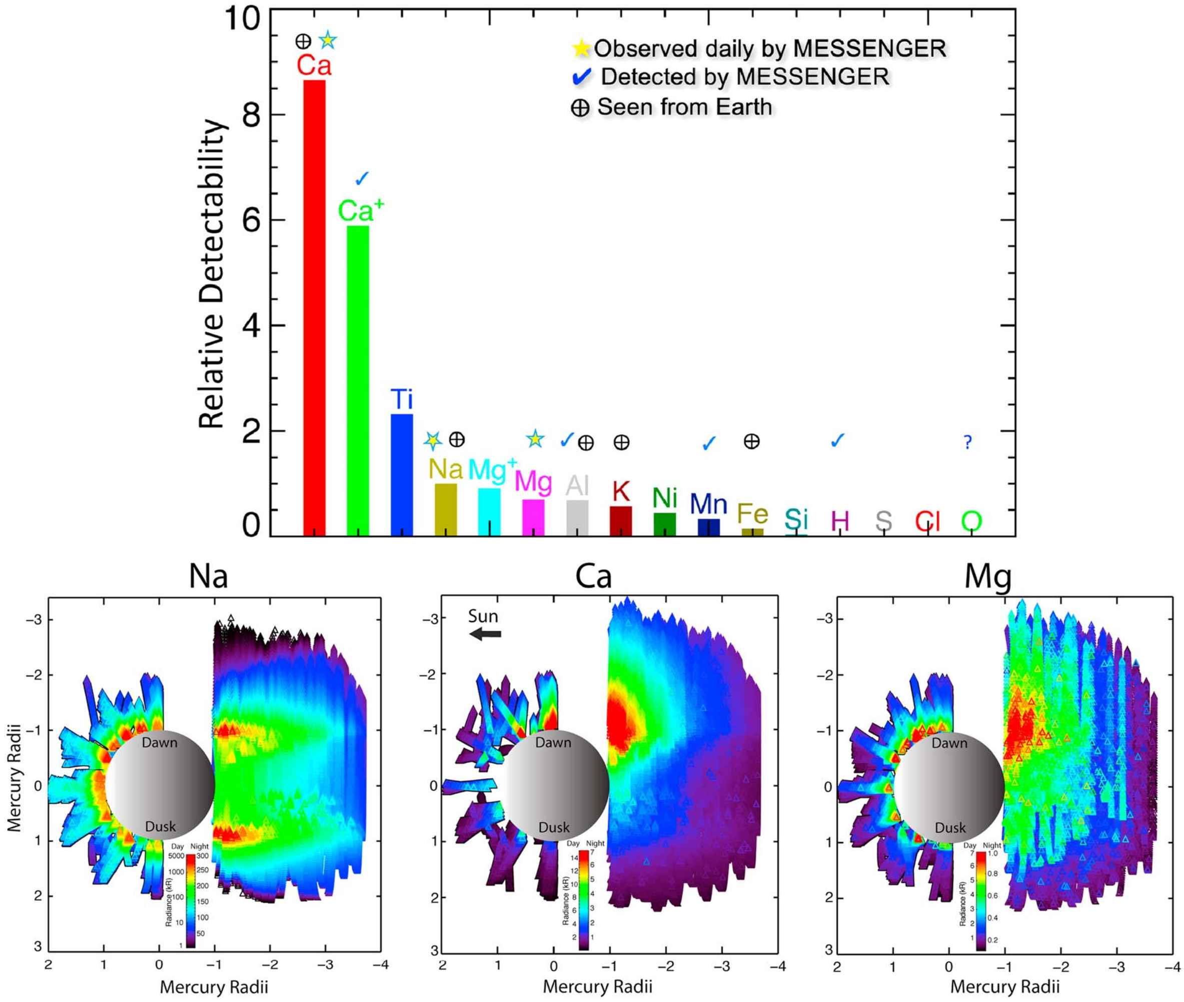


**Figure 5.** (top) Relative detectability of various exospheric species at Mercury from MESSENGER. The detectability of an individual species depends on its intrinsic emission strength and the sensitivity of the Mercury Atmospheric and Surface Composition Spectrometer instrument, and the detectability is normalized relative to that of neutral sodium [*Vervack et al.*, 2011]. (bottom) Local time distribution of from Na, Ca, and Mg emission in kR during the orbital phase of the MESSENGER mission projected into the equatorial plane. The different data coverage patterns on the dayside and nightside result from the two types of systematic observations (day side limb scans versus night side tail sweeps [*Burger et al.*, 2014; *Cassidy et al.*, 2015; *Merkel et al.*, 2016]). The color scale is specific to each species, and the dayside has a different scaling from the night side. Figure provided by A. Merkel; Mg panel from *Merkel et al.* [2016].

IMF is oppositely directed to the dayside planetary field [*Sonnerup*, 1974]. Thus, magnetic flux and plasma are transferred from the dayside to the nightside and back again more frequently and in larger amounts than at Earth [*Slavin et al.*, 2012; *DiBraccio et al.*, 2013]. Surprisingly, despite the vigorous magnetospheric dynamics, the planetary field was the dominant contribution to the magnetic field on almost all MESSENGER orbits. The long time series of observations allowed the contributions of different current systems to the quasi-steady state of the magnetosphere to be determined for the first time (Figure 4), including periodic variations in those systems related to Mercury's changing heliocentric distance [*Johnson et al.*, 2012, 2016; *Korth et al.*, 2015; *Anderson et al.*, 2014].

A major question after Mariner 10 was whether the entire dayside is ever exposed to direct solar wind impact, either because of severe compression of the magnetosphere and/or erosion of dayside magnetic flux by reconnection [*Hood and Schubert*, 1979; *Slavin and Holzer*, 1979]. MESSENGER observations have shown that this indeed can occur but is rare, occurring only about 5% of time for MESSENGER orbital observations, during extreme solar wind conditions, More typically, reconnection-driven erosion effects are offset by magnetic fields induced in the planetary core [*Slavin et al.*, 2014; *Zhong et al.*, 2015; *Johnson et al.*, 2016]. The detection

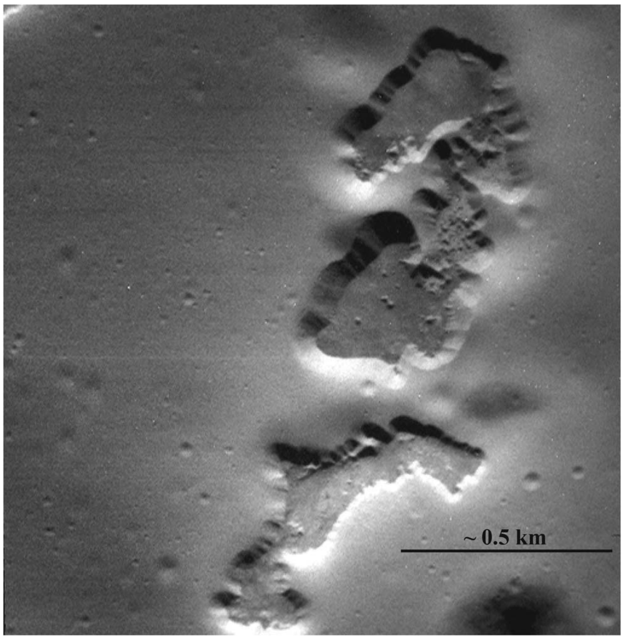


**Figure 6.** One of the highest-resolution images of hollows obtained by the Narrow Angle Camera, acquired during MESSENGER's low-altitude campaign. Image center is at 51.99°N, 272°E; the image is located within the Sholem Aleichem basin and is ~1.5 km wide. The image shows the incredibly smooth floor of these small hollows. No impact craters are visible on the floor of the hollows, even though many small craters occur on the surroundings.

of induced core fields is important because it has allowed a determination of Mercury's core radius independently of traditional geodetic techniques [*Johnson et al.*, 2016], and demonstrates that changes in solar wind conditions are sensed by the planet's iron core. Moreover, the detection of field-aligned currents and their inferred closure through the top of the outer core provides another indication that Mercury is unique in the coupling of the space environment to the deep interior [*Anderson et al.*, 2014].

MESSENGER observations have enabled substantial advances in characterization of Mercury's exosphere, complemented by many Earth-based observational campaigns and modeling efforts. The detectability of specific species is controlled by their relative emission strengths and instrument sensitivity (Figure 5). Neutral species—magnesium [*McClintock et al.*, 2009] and manganese [*Vervack et al.*, 2015]—as well as calcium ions ($Ca^+$) [*Vervack et al.*, 2010] were detected for the first time, and the presence of aluminum [*Bida and Killen*, 2016] has been confirmed. Sodium, calcium, and magnesium were observed daily, allowing their average distributions within the exosphere to be mapped (Figure 5). These distributions, and their seasonal variations, are distinct [*Burger et al.*, 2014; *Cassidy et al.*, 2015; *Merkel et al.*, 2016] suggesting different source, transport, and loss processes. For example, sodium is enhanced on the dayside and appears to be mainly produced through photon-stimulated desorption [*Cassidy et al.*, 2015]. Sodium is also enhanced near the cold-pole longitudes. Mercury's 3:2 spin-orbit resonance causes these longitudes to sit at the terminators for longer periods of each year, and because of this they are efficient sodium traps that are further filled as solar radiation pressure pushes sodium toward the nightside. When the cold poles emerge into sunlight, sodium is ejected from the surface, leading to an enhancement in emission that appears to rotate from dawn to dusk during the Mercury year. In contrast, the average distribution of calcium in the exosphere shows a substantial dawn-dusk asymmetry [*Burger et al.*, 2014]. Seasonally, the distribution of calcium tracks the flux of interplanetary dust to Mercury's surface, consistent with production through vaporization from dust impacts. Calcium production peaks sharply shortly after Mercury goes through perihelion due to an additional dust contribution from comet Encke that intersects Mercury's orbit and impacts near the dawn terminator [*Killen and Hahn*, 2015]. Magnesium also exhibits a strong dawn-dusk asymmetry, suggesting that it is primarily a result of dust impacts. However, in contrast to calcium, magnesium production shows a much broader peak shortly before perihelion with a minor peak just prior to aphelion [*Merkel et al.*, 2016]. Thus, models that adjust dust cloud properties to match the observed calcium seasonal variations cannot simultaneously explain the magnesium observations and vice versa. Notably, MESSENGER did not observe the short-term exospheric variations seen in ground-based observations, particularly for sodium [e.g., *Leblanc et al.*, 2009; *Mangano et al.*, 2013]; this discrepancy may be related to observational limitations (e.g., timing and spatial coverage) of both data sets. Collectively, the MESSENGER results suggest a highly dynamic exosphere with distinct processes governing the distributions in time and space of different species both spatially and temporally. By comparison, in situ observations of the lunar exosphere show relatively more weather in the sodium exosphere compared with at Mercury and observations of potassium indicate an enhancement over KREEP (Potassium Rare Earth Elements and Phosphorus) surface regions on the Moon [*Colaprete et al.*, 2016]. In contrast, with the exception of a possible correlation of magnesium enhancement in the exosphere with Mercury's high-magnesium surface region [*Weider et al.*, 2015], no clear links between the exosphere and surface composition have yet been identified.

Mercury's surface shows several lines of evidence for interaction with the space environment in the recent geological past. First, the high-latitude circular radar bright regions identified in Earth-based radar have been confirmed to be permanently shadowed [*Chabot et al.*, 2012] (Figure 3) and to comprise dominantly water ice [*Lawrence et al.*, 2013] that in some locations is buried beneath an insulating layer of sublimation lag [*Paige et al.*, 2013]. The observations of ice in small craters, that are challenging thermal environments for long-term ice stability, raises the question of whether the ice is relatively young. Second, the discovery of hollows (Figures 3 and 6), a geologic landform that appears to be unique to Mercury, also points to recent modification of Mercury's surface by volatiles [*Blewett et al.*, 2011, 2013; *Thomas et al.*, 2014]. These bright, small, fresh-appearing features are interpreted to be the result of geologically-recent loss of a volatile material to space. They occur dominantly in LRM, show a strong correlation with Sun-facing slopes, and are more abundant at Mercury's hot pole locations. Third, MESSENGER color and spectral data show evidence for modification of the surface by space weathering. As on the Moon, space-weathered material on Mercury is redder across the visible-to-near-infrared wavelength band than fresher material. However, because of the paucity of iron in Mercury's crust the other lunar-style diagnostic of space weathering—a decrease in the strength of the 1 μm absorption band—cannot be detected [*Murchie et al.*, 2015; *Izenberg et al.*, 2014]. In color maps of Mercury, the major spectral trend results from the difference between higher-reflectance, redder volcanic plains and pyroclastic materials versus darker, less-red LRM, with space weathering forms a secondary signature superposed on this. Geographical variations in the intensity of space weathering have not yet been identified. Whether this non-detection reflects challenges in teasing out regional variations from the data available or a time-integrated space weathering signature that is relatively uniform globally, and not for example, stronger in the high-latitude magnetic field cusp regions, is unknown.

## 4. Next Steps

MESSENGER has revealed a whole new Mercury to discover. Its bounty of data provides ample opportunity to deeply investigate enduring and unanticipated avenues. With the next spacecraft to visit Mercury set to arrive in the mid-2020s, MESSENGER data will represent the best data set for studying Mercury for almost a decade to come. The opportunities for understanding Mercury and its place in the Solar System brought to light by MESSENGER are too many to name. However, we can highlight a few of the most critical questions and paths to greater discovery.

The question of whether Mercury has a history of volcanism has been clearly settled [e.g., *Head et al.*, 2011; *Denevi et al.*, 2013]. Yet the understanding of the evolution of volcanism on the planet and what that history implies about processes in the interior are at an early stage. Volcanism is a reflection of conditions in the interior and thus constraining the timing, the distribution, and importantly, the compositions of volcanism are critical to understanding the planet as a whole. One vitally important way to make progress on how volcanism varies and has evolved on Mercury is to collect geochemical and mineralogical information at geologically relevant spatial scales. Collecting such detailed information on a global scale will provide the opportunity to understand the sources and geological relationships of geochemical variability on the surface [e.g., *Peplowski et al.*, 2012; *Weider et al.*, 2015].

High spatial resolution compositional mapping of the surface will also be critical for understanding the nature of hollows [e.g., *Blewett et al.*, 2011, 2013; *Thomas et al.*, 2014, 2016]. Constraining the thickness and composition of the materials in and around the hollows may point to how these features form and why they are most often associated with impact craters. The role of volatile materials in producing hollows is particularly tantalizing, as it could provide a constraint on the near-surface volatile inventory of the planet.

A related, but distinct issue is further study of the polar deposits, in particular further constraints on their composition and thickness. These deposits are an important record of water delivery and movement in the solar system. Substantial advances could be made through in situ characterization of the deposit material and its thermo-physical environment.

Global geochemical and mineralogical information at consistent spatial scales is crucial for understanding the bulk composition and development of Mercury's crust. Spatially resolved major element information on the southern hemisphere is limited [*Weider et al.*, 2015], and mineralogical information is lacking. Further constraints on the genesis of Mercury's fractionally thick crust will depend upon chemical and mineralogical information capable of elucidating more completely the degrees and source(s) of melting. Another avenue of investigation is narrowing the plausible suite of carriers of crustal magnetization, as this in turn provides further information on the iron mineralogy of the crust. More complete gravity and topography information, to higher spatial resolution across the planet and especially in the southern hemisphere, will permit more robust estimates of the thickness of the crust and how it varies across the planet [e.g., *James et al.*, 2015; *Padovan et al.*, 2015].

MESSENGER confirmed the existence of Mercury's liquid outer core and elucidated the planet's basic internal structure [e.g., *Smith et al.*, 2012]. The structure within the core, including the presence and size of a solid inner core and any indication of top-down crystallization (iron snow), remains to be determined. Mercury's magnetic field structure and strength are products of processes occurring within the metallic core and the boundary conditions set by its structure. A related problem that requires multiple types of investigation is the temporal evolution of Mercury's dynamo field—was this intermittent or continuous? Refinement of the rotational state of the planet and its tidal response offers opportunities to place limits on the structure of the core. However, detailed understanding of the structure will ultimately require seismological determination of interior properties, in particular the size of the inner core and any evidence for density layering in the outer core.

Progress in understanding Mercury's magnetosphere and exosphere, and couplings among these and the planet's surface and interior require simultaneous in situ measurements of the solar wind driving conditions and the magnetospheric/exospheric response. An important characteristic time scale for magnetospheric dynamics, the Dungey cycle [*Dungey*, 1961], is on the order of a few minutes at Mercury, compared with several hours at Earth. MESSENGER's orbital period was much longer than the time scale for these dynamics, and so independent, simultaneous measurements of the solar wind driving conditions and the magnetospheric response could not be made. In this regard, the Bepi-Colombo mission with its dual orbiters, one of which will be dominantly inside and one outside the magnetosphere, will make important and substantive progress. Magnetic sounding of the planetary interior at a variety of frequencies will allow the electrical conductivity structure of the mantle to be probed; this in turn is a strong constraint on the present-day mantle thermal structure. Improved mapping of the planetary field in the southern hemisphere by the lower altitude Bepi-Colombo spacecraft will be important for constraining the global core field structure and hence dynamo models. Detection of the southern hemisphere cusp region, in particular its spatial extent relative to its northern hemisphere counterpart, is relevant to space weathering studies and the production of exospheric species [*Anderson et al.*, 2011]. Improved measurements of exospheric species, together with higher-resolution surface compositional information, would allow links between the exosphere and surface composition to be investigated.

MESSENGER's exploration of Mercury has, unsurprisingly, extended existing lines of inquiry and opened novel ones. A clear thread is that while MESSENGER has enabled a new view of the innermost planet, in many ways this was a reconnaissance mission, setting the stage for much-needed future exploration. The next steps in answering these questions will require both new work in laboratories here on Earth and further detailed examination at Mercury.

**Acknowledgments**
We gratefully acknowledge the engineering team and the Principal Investigator, Sean C. Solomon, whose collective efforts over almost two decades enabled the incredible accomplishments of the MESSENGER mission. This paper is dedicated to the memory of Stan Peale and Mario Acuña whose efforts paved the way for fundamental discoveries regarding Mercury's present interior state. The MESSENGER mission was supported by the NASA Discovery Program, under contracts NAS5-97271 to The Johns Hopkins University Applied Physics Laboratory and NASW-00002 to the Carnegie Institution of Washington, as well as the MESSENGER Participating Scientist Program. C.L.J. also acknowledges support from the Natural Sciences and Engineering Research Council of Canada. S.A.H. also acknowledges support from the NASA Solar System Workings Program grant NNX15AH31G. We thank Tim Cassidy, Bill McClintock, Aimee Merkel, and Ron Vervack for their input on the exosphere discussion and for their assistance with Figure 5. We thank J. Halekas and P. James for their constructive reviews that helped improve the manuscript. All data discussed in this paper are available in the cited references, and the MESSENGER data that supports that work is publicly available at the NASA Planetary Data System (https://pds.nasa.gov).

## References

Aharonson, O., M. T. Zuber, and S. C. Solomon (2004), Crustal remanence in an internally magnetized non-uniform shell: A possible source for Mercury's magnetic field?, *Earth Planet. Sci. Lett.*, *218*, 261–268, doi:10.1016/s0012-821x(03)00682-4.

Anderson, B. J., M. H. Acuna, H. Korth, M. E. Purucker, C. L. Johnson, J. A. Slavin, S. C. Solomon, and R. L. McNutt (2008), The structure of Mercury's magnetic field from MESSENGER's first flyby, *Science*, *321*, 82–85.

Anderson, B. J., C. L. Johnson, H. Korth, M. E. Purucker, R. M. Winslow, J. A. Slavin, S. C. Solomon, R. L. McNutt Jr., J. M. Raines, and T. H. Zurbuchen (2011), The global magnetic field of Mercury from MESSENGER orbital observations, *Science*, *333*, 1859–1862, doi:10.1126/science.1211001.

Anderson, B. J., C. L. Johnson, H. Korth, R. M. Winslow, J. E. Borovsky, M. E. Purucker, J. A. Slavin, S. C. Solomon, M. T. Zuber, and R. L. McNutt (2012), Low-degree structure in Mercury's planetary magnetic field, *J. Geophys. Res.*, *117*, E00L12, doi:10.1029/2012JE004159.

Anderson, B. J., C. L. Johnson, H. Korth, J. A. Slavin, R. M. Winslow, R. J. Phillips, R. L. McNutt Jr., and S. C. Solomon (2014), Steady-state field-aligned currents at Mercury, *Geophys. Res. Lett.*, *41*, 7444–7452, doi:10.1002/2014GL061677.

Bida, T., and R. M. Killen (2016), Observations of the minor species Al and Fe in Mercury's exosphere, *Icarus*, doi:10.1016/j.icarus.2016.10.019.
Blewett, D. T., et al. (2011), Hollows on Mercury: MESSENGER evidence for geologically recent volatile-related activity, *Science*, *333*, 1856–1859, doi:10.1126/science.1211681.
Blewett, D. T., et al. (2013), Mercury's hollows: Constraints on formation and composition from analysis of geological setting and spectral reflectance, *J. Geophys. Res. Planets*, *118*, 1013–32, doi:10.1029/2012JE004174.
Broadfoot, A. L., S. Kumar, M. J. Belton, and M. B. McElroy (1974), Mercury's atmosphere from Mariner 10: Preliminary results, *Science*, *185*, 166–169.
Brown, S. M., and L. T. Elkins-Tanton (2009), Compositions of Mercury's earliest crust from magma ocean models, *Earth Planet. Sci. Lett.*, *286*, 446–455.
Burger, M. H., R. M. Killen, W. E. McClintock, A. W. Merkel, R. J. Vervack, T. A. Cassidy, and M. Sarantos (2014), Seasonal variations in Mercury's dayside calcium exosphere, *Icarus*, *238*, 51–58, doi:10.1016/j.icarus.2014.04.049.
Butler, B. J., D. O. Muhleman, and M. A. Slade (1993), Mercury: Full-disk radar images and the detection and stability of ice at the north pole, *J. Geophys. Res.*, *98*, 15,003–15,023, doi:10.1029/93JE01581.
Byrne, P. K., C. Klimczak, A. M. C. Şengör, S. C. Solomon, T. R. Watters, and S. A. Hauck II (2014), Mercury's global contraction much greater than earlier estimates, *Nat. Geosci.*, *7*, 301–307, doi:10.1038/ngeo2097.
Byrne, P. K., L. R. Ostrach, C. I. Fassett, C. R. Chapman, B. W. Denevi, A. J. Evans, C. Klimczak, M. E. Banks, J. W. Head, and S. C. Solomon (2016), Widespread effusive volcanism on Mercury likely ended about 3.5 Ga, *Geophys. Res. Lett.*, *43*, 7408–7416, doi:10.1002/2016GL069412.
Cao, H., J. M. Aurnou, J. Wicht, W. Dietrich, K. M. Soderlund, and C. T. Russell (2014), A dynamo explanation for Mercury's anomalous magnetic field, *Geophys. Res. Lett.*, *41*, 4127–4134, doi:10.1002/2014GL060196.
Cassidy, T. A., A. W. Merkel, M. H. Burger, M. Sarantos, R. M. Killen, W. E. McClintock, and R. J. Vervack Jr. (2015), Mercury's seasonal sodium exosphere: MESSENGER orbital observation, *Icarus*, *248*, 547–559.
Chabot, N. L., Ernst, C. M., Denevi, B. W., Harmon, J. K., Murchie, S. L., Blewett, D. T., Solomon, S. C., and Zhong, E. D. (2012), Areas of permanent shadow in Mercury's south polar region ascertained by MESSENGER orbital imaging, *Geophys. Res. Lett.*, *39*, L09204, doi:10.1029/2012GL051526.
Chabot, N. L., E. A. Wollack, R. L. Klima, and M. E. Minitti (2014), Experimental constraints on Mercury's core composition, *Icarus*, *390*, 199–208, doi:10.1016/j.epsl.2014.01.004.
Charlier, B., T. L. Grove, and M. T. Zuber (2013), Phase equilibria of ultramafic compositions on Mercury and the origin of the compositional dichotomy, *Earth Planet. Sci. Lett.*, *363*, 50–60, doi:10.1016/j.epsl.2012.12.021.
Colaprete, A., M. Sarantos, D. H. Wooden, T. J. Stubbs, A. M. Cook, and M. Shirley (2016), How surface composition and meteoroid impacts mediate sodium and potassium in the lunar exosphere, *Science*, *351*, 249–252, doi:10.1126/science.aad2380.
Connerney, J. E. P., and N. F. Ness (1988), Mercury's magnetic field and interior, in *Mercury*, edited by F. Vilas, C. R. Chapman, and M. S. Matthews, pp. 494–513, Univ. of Arizona Press, Tucson.
Denevi, B. W., et al. (2009), The evolution of Mercury's crust: A global perspective from MESSENGER, *Science*, *324*, 613–618.
Denevi, B. W., et al. (2013), The distribution and origin of smooth plains on Mercury, *J. Geophys. Res. Planets*, *118*, 891–907, doi:10.1002/jgre.20075.
Deutsch, A. N., N. L. Chabot, E. Mazarico, C. M. Ernst, J. W. Head, G. A. Neumann, and S. C. Solomon (2016), Comparison of areas in shadow from imaging and altimetry in the north polar region of Mercury and implications for polar ice deposits, *Icarus*, *280*, 158–171.
DiBraccio, G. A., J. A. Slavin, S. A. Boardsen, B. J. Anderson, H. Korth, T. H. Zuburchen, J. M. Raines, D. N. Baker, R. L. McNutt Jr., and S. C. Solomon (2013), MESSENGER observations of magnetopause structure and dynamics at Mercury, *J. Geophys. Res. Space Physics*, *118*, 997−1008, doi:10.1002/jgra.50123.
Dungey, J. W. (1961), Interplanetary magnetic field and the auroral zones, *Phys. Rev. Lett.*, *6*, 47–48, doi:10.1103/PhysRevLett.6.47.
Harder, H., and G. Schubert (2001), Sulfur in Mercury's core?, *Icarus*, *151*, 118–122, doi:10.1006/icar.2001.6586.
Harmon, J. K., and M. A. Slade (1992), Radar mapping of Mercury: Full-disk images and polar anomalies, *Science*, *258*, 640–643.
Harmon, J. K., M. A. Slade, and M. S. Rice (2011), Radar imagery of Mercury's putative polar ice: 1999–2005 Arecibo results, *Icarus*, *211*, 37–50.
Hauck, S. A., II, A. J. Dombard, R. J. Phillips, and S. C. Solomon (2004), Internal and tectonic evolution of Mercury, *Earth Planet. Sci. Lett.*, *222*, 713–728, doi:10.1016/j.epsl.2004.03.037.
Hauck, S. A. II, S. C. Solomon, and D. A. Smith (2007), Predicted recovery of Mercury's internal structure by MESSENGER, *Geophys. Res. Lett.*, *34*, L18201, doi:10.1029/2007GL030793.
Hauck, S. A., II, et al. (2013), The curious case of Mercury's internal structure, *J. Geophys. Res. Planets*, *118*, 1204–1220, doi:10.1002/jgre.20091.
Head, J. W., III, et al. (2011), Flood volcanism in the northern high latitudes of Mercury revealed by MESSENGER, *Science*, *333*, 1853–1856, doi:10.1126/science.1211997.
Hood, L. L. (2015), Initial mapping of Mercury's crustal magnetic field: Relationship to the Caloris impact basin, *Geophys. Res. Lett.*, *42*, 10,565–10,572, doi:10.1002/2015GL066451.
Hood, L. L. (2016), Magnetic anomalies concentrated near and within Mercury's impact basins: Early mapping and interpretation, *J. Geophys. Res. Planets*, *121*, 1016–1025, doi:10.1002/2016JE005048.
Hood, L. L., and G. Schubert (1979), Inhibition of solar wind impingement on Mercury by planetary induction currents, *J. Geophys. Res.*, *84*, 2641–2647, doi:10.1029/JA084iA06p02641.
Ingersoll, A. P., T. Svitek, and B. C. Murray (1992), Stability of polar frosts in spherical bowl-shaped craters on Moon, Mercury, and Mars, *Icarus*, *100*, 40–47.
Izenberg, N. R., et al. (2014), The low-iron, reduced surface of Mercury as seen in spectral reflectance by MESSENGER, *Icarus*, *228*, 364–374.
James, P. B., M. T. Zuber, R. J. Phillips, and S. C. Solomon (2015), Support of long-wavelength topography on Mercury inferred from MESSENGER measurements of gravity and topography, *J. Geophys. Res. Planets*, *120*, 287–310, doi:10.1002/2014JE004713.
Johnson, C. L., et al. (2012), MESSENGER observations of Mercury's magnetic field structure, *J. Geophys. Res.*, *117*, E00L14, doi:10.1029/2012JE004217.
Johnson, C. L., et al. (2015), Low-altitude magnetic field measurements by MESSENGER reveal Mercury's ancient crustal field, *Science*, *348*, 892–895, doi:10.1126/science.aaa8720.
Johnson, C. L., L. C. Philpott, B. J. Anderson, H. Korth, S. A. Hauck II, D. Heyner, R. J. Phillips, R. M. Winslow, and S. C. Solomon (2016), MESSENGER observations of induced magnetic fields in Mercury's core, *Geophys. Res. Lett.*, *43*, 2436–2444, doi:10.1002/2015GL067370.
Killen, R. M., and J. M. Hahn (2015), Impact Vaporization as a Possible Source of Mercury's Calcium Exosphere, *Icarus*, *250*, 230–237, doi:10.1016/j.icarus.2014.11.035.
Knibbe, J. S., and W. van Westrenen (2015), The interior configuration of planet Mercury constrained by moment of inertia and planetary contraction, *J. Geophys. Res. Planets*, *120*, 1904–1923, doi:10.1002/2015JE004908.

Korth, H., N. A. Tsyganenko, C. L. Johnson, L. C. Philpott, B. J. Anderson, M. M. Al Asad, S. C. Solomon, and R. L. McNutt Jr. (2015), Modular model for Mercury's magnetospheric magnetic field confined within the average observed magnetopause, *J. Geophys. Res. Spcae Physics*, *120*, 4503–4518, doi:10.1002/2015JA021022.

Lawrence, D. J., et al. (2013), Evidence for water ice near Mercury's north pole from MESSENGER Neutron Spectrometer measurements, *Science*, *339*, 292–296, doi:10.1126/science.1229953.

Leblanc, F., A. Doressoundiram, N. M. Schneider, S. Massetti, M. Wedlund, A. Lopez Ariste, C. Barbieri, V. Mangano, and G. Cremonese (2009), Short-term variations of Mercury's Na exosphere observed with very high spectral resolution, *Geophys. Res. Lett.*, *36*, L07201, doi:10.1029/2009GL038089.

Lillis, R. J., H. V. Frey, and M. Manga (2008), Rapid decrease in Martian crustal magnetization in the Noachian era: Implications for the dynamo and climate of early Mars, *Geophys. Res. Lett.*, *35*, L14203, doi:10.1029/2008GL034338.

Mangano, V., S. Massetti, A. Milillo, A. Mura, S. Orsini, and F. Leblanc (2013), Dynamical evolution of sodium anisotropies in the exosphere of Mercury, *Planet. Space Sci.*, *82–83*, 1–10, doi:10.1016/j.pss.2013.03.002.

Marchi, S., C. R. Chapman, C. I. Fassett, J. W. Head, W. F. Bottke, and R. G. Strom (2013), Global resurfacing of Mercury 4.0–4.1 billion years ago by heavy bombardment and volcanism, *Nature*, *499*, 59–61, doi:10.1038/nature12280.

McClintock, W. E., R. J. Vervack, E. T. Bradley, R. M. Killen, N. Mouawad, A. L. Sprague, M. H. Burger, S. C. Solomon, and N. R. Izenberg (2009), MESSENGER observations of Mercury's exosphere: Detection of magnesium and distribution of constituents, *Science*, *324*, 610–613, doi:10.1126/science.1172525.

McKinnon, W. B., K. J. Zahnle, B. A. Ivanov, and H. J. Melosh (1997), Cratering on Venus: Models and observations, in *Venus II*, edited by S. W. Bougher, D. M. Hunten, and R. J. Phillips, pp. 969–1014 , Univ. of Arizona Press, Tucson.

Merkel, A. W., T. A. Cassidy, R. J. Vervack Jr., W. E. McClintock, M. Sarantos, M. H. Burger, and R. M. Killen (2016), Seasonal variations of Mercury's magnesium dayside exosphere from MESSENGER observations, *Icarus*, *281*, 46–54, doi:10.1016/j.icarus.2016.08.032.

Michel, N. C., S. A. Hauck, S. C. Solomon, R. J. Phillips, J. H. Roberts, and M. T. Zuber (2013), Thermal evolution of Mercury as constrained by MESSENGER observations, *J. Geophys. Res. Planets*, *118*, 1033–1044, doi:10.1002/jgre.20049.

Murchie, S. L., et al. (2015), Orbital multispectral mapping of Mercury with the MESSENGER Mercury Dual Imaging System: Evidence for the origins of plains units and low-reflectance material, *Icarus*, *254*, 287–305, doi:10.1016/j.icarus.2015.03.027.

Namur, O., M. Collinet, B. Charlier, T. L. Grove, F. Holtz, and C. McCammon (2016), Melting processes and mantle sources of lavas on Mercury, *Earth Planet. Sci. Lett.*, *439*, 117–128, doi:10.1016/j.epsl.2016.01.030.

Ness, N. F., K. W. Behannon, R. P. Lepping, Y. C. Whang, and K. H. Schatten (1974), Magnetic field observations near Mercury: Preliminary results from Mariner 10, *Science*, *185*, 151–160.

Nimmo, F. (2002), Constraining the crustal thickness on Mercury from viscous topographic relaxation, *Geophys. Res. Lett.*, *29*(5), 1063, doi:10.1029/2001GL013883.

Nimmo, F., and T. R. Watters (2004), Depth of faulting on Mercury: Implications for heat flux and crustal and effective elastic thickness, *Geophys. Res. Lett.*, *31*, L02701, doi:10.1029/2003GL018847.

Nittler, L. R., et al. (2011), The major-element composition of Mercury's surface from MESSENGER X-ray spectrometry, *Science*, *333*, 1847–1850, doi:10.1126/science.1211567.

Ostrach, L. R., M. S. Robinson, J. L. Whitten, C. I. Fassett, R. G. Strom, J. W. Head, and S. C. Solomon (2015), Extent, age, and resurfacing history of the northern smooth plains on Mercury from MESSENGER observations, *Icarus*, *250*, 602–622, doi:10.1016/j.icarus.2014.11.010.

Padovan, S., J.-L. Margot, S. A. Hauck, W. B. Moore, and S. C. Solomon (2014), The tides of Mercury and possible implications for its interior structure, *J. Geophys. Res. Planets*, *119*, 850–866, doi:10.1002/2013JE004459.

Padovan, S., M. A. Wieczorek, J.-L. Margot, N. Tosi, and S. C. Solomon (2015), Thickness of the crust of Mercury from geoid-to-topography ratios, *Geophys. Res. Lett.*, *42*, 1029–1038, doi:10.1002/2014GL062487.

Paige, D. A., S. E. Wood, and A. R. Vasavada (1992), The thermal stability of water ice at the poles of Mercury, *Science*, *258*, 643–646.

Paige, D. A., M. A. Siegler, J. K. Harmon, G. A. Neumann, E. M. Mazarico, D. E. Smith, M. T. Zuber, E. Harju, M. L. Delitsky, and S. C. Solomon (2013), Thermal stability of volatiles in the north polar region of Mercury, *Science*, *339*, 300–303.

Peale, S. J., J.-L. Margot, S. A. Hauck, II, and S. C. Solomon (2016), Consequences of an inner core on Mercury's spin configuration, *Icarus*, *264*, 443–455.

Peplowski, P. N., et al (2011), Radioactive elements on Mercury's surface from MESSENGER: Implications for the planet's formation and evolution, *Science*, *333*, 1850–1852, doi:10.1126/science.1211576.

Peplowski, P. N., et al. (2012), Variations in the abundances of potassium and thorium on the surface of Mercury: Results from the MESSENGER Gamma-Ray Spectrometer, *J. Geophys. Res.*, *117*, E00L04, doi:10.1029/2012JE004141.

Peplowski, P. N., R. L. Klima, D. J. Lawrence, C. M. Ernst, B. W. Denevi, E. A. Frank, J. O. Goldsten, S. L. Murchie, L. R. Nittler, and S. C. Solomon (2016), Remote sensing evidence for an ancient carbon-bearing crust on Mercury, *Nat. Geosci.*, *9*, 273–276, doi:10.1038/ngeo2669.

Pettengill, G. H., and R. B. Dyce (1965), A radar determination of the rotation of the planet Mercury, *Nature*, *206*, 451–2.

Potter, A. E., and T. H. Morgan (1985), Discovery of sodium in the atmosphere of Mercury, *Science*, *229*, 651–653, doi:10.1126/science.229.4714.651.

Potter, A. E., and T. H. Morgan (1986), Potassium in the atmosphere of Mercury, *Icarus*, *67*, 336–340.

Prockter, L. M., et al. (2010), Evidence for young volcanism on Mercury from the third MESSENGER flyby, *Science*, *329*, 668–671, doi:10.1126/science.1188186.

Rivoldini, A., and T. Van Hoolst (2013), The interior structure of Mercury constrained by the low-degree gravity field and the rotation of Mercury, *Earth Planet. Sci. Lett.*, *377-378*, 62–72, doi:10.1016/j.epsl.2013.07.021.

Russell, C. T., D. N. Baker, and J. A. Slavin (1988), The magnetosphere of Mercury, in *Mercury*, edited by F. Vilas, C. R. Chapman, and M. S. Matthews, pp. 514–561, Univ. of Arizona Press, Tuscon, AZ.

Schubert, G., M. N. Ross, D. J. Stevenson, and T. Spohn (1988), Mercury's thermal history and the generation of its magnetic field, in *Mercury*, edited by F. Vilas, C. R. Chapman, and M. S. Matthews, pp. 429–460, Univ. of Arizona Press, Tucson.

Slade, M. A., B. J. Butler, and D. O. Muhleman (1992), Mercury radar imaging—Evidence for polar ice, *Science*, *258*, 635–640.

Slavin, J. A., and R. E. Holzer (1979), The effect of erosion on the solar wind stand-off distance at Mercury, *J. Geophys. Res.*, *84*, 2076–2082, doi:10.1029/JA084iA05p02076.

Slavin, J. A., et al. (2012), MESSENGER and Mariner 10 flyby observations of magnetotail structure and dynamics at Mercury, *J. Geophys. Res.*, *117*, A01215, doi:10.1029/2011JA016900.

Slavin, J. A., et al. (2014), MESSENGER observations of Mercury's dayside magnetosphere under extreme solar wind conditions, *J. Geophys. Res. Space Physics*, *119*, 8087–8116, doi:10.1002/2014JA020319.

Smith, D. E., et al. (2012), Gravity field and internal structure of Mercury from MESSENGER, *Science*, *336*, 214–217.

Solomon, S. C. (1977), The relationship between crustal tectonics and internal evolution in the Moon and Mercury, *Phys. Earth Planet. Inter.*, *15*, 135–145.
Sonnerup, B. U. Ö. (1974), Magnetopause reconnection rate, *J. Geophys. Res.*, *79*, 1546–1549, doi:10.1029/JA079i010p01546.
Stanley, S., and G. A. Glatzmaier (2010), Dynamo models for planets other than, *Earth Space Sci. Rev.*, *152*, 617–649, doi:10.1007/s11214-009-9573-y.
Stockstill-Cahill, K. R., T. J. McCoy, L. R. Nittler, S. Z. Weider, and S. A. Hauck II (2012), Magnesium-rich crustal compositions on Mercury: Implications for magmatism from petrologic modeling, *J. Geophys. Res.*, *117*, E00L15, doi:10.1029/2012JE004140.
Strom, R. G., N. J. Trask, and J. E. Guest (1975), Tectonism and volcanism on Mercury, *J. Geophys. Res.*, *80*, 2478–2507, doi:10.1029/JB080i017p02478.
Taylor, G. J., and E. R. D. Scott (2003), Mercury, in *Treatise on Geochemistry*, edited by H. D. Holland and K. K. Turekian, pp. 477–485, Pergamon, Oxford.
Thomas, R. J., D. A. Rothery, S. J. Conway, and M. Anand (2014), Hollows on Mercury: Materials and mechanisms involved in their formation, *Icarus*, *229*, 221–35, doi:10.1016/j.icarus.2013.11.018.
Thomas, R. J., B. M. Hynek, D. A. Rothery, and S. J. Conway (2016), Mercury's low-reflectance material: Constraints from hollows, *Icarus*, *277*, 455–465, doi:10.1016/j.icarus.2016.05.036.
Tian, Z., M. T. Zuber, and S. Stanley (2015), Magnetic field modeling for Mercury using dynamo models with a stable layer and laterally variable heat flux, *Icarus*, *260*, 263–268, doi:10.1016/j.icarus.2015.07.019.
Tosi, N., M. Grott, A. C. Plesa, and D. Breuer (2013), Thermochemical evolution of Mercury's interior, *J. Geophys. Res. Planets*, *118*, 2474–2487, doi:10.1002/jgre.20168.
Vander Kaaden, K. E., and F. M. McCubbin (2015), Exotic crust formation on Mercury: Consequences of a shallow, FeO-poor mantle, *J. Geophys. Res. Planets*, *120*, 195–209, doi:10.1002/2014JE004733.
Vervack, R. J., W. E. McClintock, R. M. Killen, A. L. Sprague, B. J. Anderson, M. H. Burger, E. T. Bradley, N. Mouawad, S. C. Solomon, and N. R. Izenberg (2010), Mercury's complex exosphere: Results from MESSENGER's third flyby, *Science*, *329*, 672–675, doi:10.1126/science.1188572.
Vervack, R. J. Jr., W. E. McClintock, R. M. Killen, A. L. Sprague, M. H. Burger, A. W. Merkel, and M. Sarantos (2011), Early MESSENGER results for less abundant or weakly emitting species in Mercury's exosphere, EPSC-DPS Joint Meeting, Abstract 1131.
Vervack, R. J. Jr., W. E. McClintock, R. M. Killen, A. W. Merkel, M. H. Burger, M. Sarantos, and T. A. Cassidy (2015), Mercury's exosphere: New detections, discoveries, and insights, paper presented at the 47th Annual Meeting of the Division for Planetary Sciences, National Harbor, Maryland, November 8-13.
Watters, T. R., M. S. Robinson, and A. C. Cook (1998), Topography of lobate scarps on Mercury: New constraints on the planet's contraction, *Geology*, *26*, 991–994.
Weider, S. Z., et al. (2015), Evidence for geochemical terranes on Mercury: Global mapping of major elements with MESSENGER's X-Ray Spectrometer, *Earth Planet. Sci. Lett.*, *416*, 109–120, doi:10.1016/j.epsl.2015.01.023.
Weiss, B. P., and S. M. Tikoo (2014), The lunar dynamo, *Science*, *346*, 1198, doi:10.1126/science.1246753.
Wilhelms, D. E. (1976), Mercurian volcanism questioned, *Icarus*, *28*, 551–558.
Wood, J. A., J. S. Dickey Jr., U. B. Marvin, and B. J. Powell (1970), Lunar anorthosites and a geophysical model of the Moon, *Proc. Apollo 11 Lunar Sci. Conf.*, *1*, 965–988.
Zhong, J., W. X. Wan, Y. Wei, J. A. Slavin, J. M. Raines, Z. J. Rong, L. H. Chai, and X. H. Han (2015), Compressibility of Mercury's dayside magnetosphere, *Geophys. Res. Lett.*, *42*, 10,135–10,139, doi:10.1002/2015GL067063.